

低共熔溶剂中超疏水结构的一步 电沉积制备及性能研究

李梦情¹, 崔偎偎¹, 白子龙¹, 徐银杏¹, 于会珠¹, 李瑞乾^{1,2*}

(1. 阜阳师范大学 化学与材料工程学院, 安徽 阜阳 236037;

2. 生物质转化与污染防治安徽省高校工程技术研究中心, 安徽 阜阳 236037)

摘要: **目的** 实现电沉积镀层表面微纳分级结构的简单构筑, 赋予其优异的超疏水特性。 **方法** 以氯化胆碱-尿素低共熔溶剂为溶剂, 加入一定比例的氯化镍和硬脂酸溶解后得到电解液, 通过调节电沉积时间得到一系列不同形貌的硬脂酸镍镀层。利用 SEM、FTIR 和 XPS 等表征技术研究了沉积时间对所制备镀层形貌和组成的影响, 利用接触角测量仪探究了不同形貌硬脂酸镍的超疏水性和化学稳定性, 利用电化学工作站考察了超疏水镀层的耐腐蚀性。 **结果** 在低共熔溶剂中通过一步电沉积法得到不同形貌结构的硬脂酸镍镀层, 其表面形貌与沉积时间密切相关。沉积初期呈现纳米片状结构, 随着沉积进行, 硬脂酸镍纳米片逐渐堆积、交叉, 最终形成花状微纳分级结构。得益于其独特的微纳分级结构和自身低表面能特性, 花状硬脂酸镍镀层不仅具有优异的超疏水性 ($\theta_{\text{WCA}}=(157.3\pm 1.9)^{\circ}$, $\theta_{\text{SA}}=(3.6\pm 1.1)^{\circ}$) 和自清洁特性, 还对强酸、强碱以及盐溶液表现出优异的化学稳定性。与纳米片状和零散花状的硬脂酸镍相比, 花状微纳分级结构的硬脂酸镍的耐腐蚀性 ($J_{\text{corr}}=1.75\times 10^{-6}\text{ A/cm}^2$) 分别提高了 20 倍和 7 倍。 **结论** 以低共熔溶剂为电解液, 通过控制沉积时间可实现镀层表面微纳分级结构的调控与构筑, 进而获得性能优异的超疏水镀层。

关键词: 低共熔溶剂; 电沉积; 硬脂酸镍; 微纳分级结构; 超疏水; 耐腐蚀; 自清洁

中图分类号: TG174; TB34 **文献标识码:** A **文章编号:** 1001-3660(2023)09-0331-09

DOI: 10.16490/j.cnki.issn.1001-3660.2023.09.029

One-step Electrodeposition and Performance of Superhydrophobic Structure from Deep Eutectic Solvent

LI Meng-qing¹, CUI Wei-wei¹, BAI Zi-long¹, XU Yin-xing¹, YU Hui-zhu¹, LI Rui-qian^{1,2*}

(1. School of Chemistry and Materials Engineering, Fuyang Normal University, Anhui Fuyang 236037, China;

2. Engineering Research Centre of Biomass Conversion and Pollution Prevention Control of Anhui Provincial Department of Education, Anhui Fuyang 236037, China)

ABSTRACT: In this work, a template free one-step electrodeposition method in deep eutectic solvent (DES) was reported for

收稿日期: 2022-07-05; 修订日期: 2022-11-25

Received: 2022-07-05; Revised: 2022-11-25

基金项目: 国家自然科学基金 (52101080); 安徽高校优秀青年科研项目 (2022AH030132); 安徽省自然科学基金 (2008085QE201、2008085QB54); 安徽省高校自然科学研究项目 (KJ2020A0537、2022AH051316); 阜阳师范大学青年人才重点项目 (rcxm202207、2017KYQD0009); 大学生创新创业项目 (202110371003、S202210371045)

Fund: Supported by the National Natural Science Foundation of China (52101080); College Excellent Young Foundation of Anhui Province (2022AH030132); Natural Science Foundation of Anhui Province (2008085QE201, 2008085QB54); Project of Natural Science Research in University of Anhui Province (KJ2020A0537, 2022AH051316); Young Talent Foundation of Fuyang Normal University (rcxm202207, 2017KYQD0009); Training Program for College Students' Innovation and Entrepreneurship (202110371003, S202210371045)

引文格式: 李梦情, 崔偎偎, 白子龙, 等. 低共熔溶剂中超疏水结构的一步电沉积制备及性能研究[J]. 表面技术, 2023, 52(9): 331-339.

LI Meng-qing, CUI Wei-wei, BAI Zi-long, et al. One-step Electrodeposition and Performance of Superhydrophobic Structure from Deep Eutectic Solvent[J]. Surface Technology, 2023, 52(9): 331-339.

the preparation of hierarchical structured superhydrophobic surface with excellent chemical stability, corrosion resistance and self-cleaning properties. It is well known that, surface hierarchical structures and surface free energy are the main factors for preparation of superhydrophobic surfaces. To fabricate the superhydrophobic surface with micro/nano hierarchical structures by one-step electrodeposition, in this paper, the choline chloride-urea deep eutectic solvent (ChCl-Urea DES) containing 0.04 mol/L $\text{NiCl}_2 \cdot 6\text{H}_2\text{O}$ and 0.1 mol/L stearic acid was used as electrolyte. A series of nickel stearate ($\text{Ni}[\text{CH}_3(\text{CH}_2)_{16}\text{COO}]_2$) coatings with different surface morphologies were obtained on the copper substrate by regulating the electrodeposition time (These coatings were named NS-1, NS-2 and NS-3 based on the deposition time, respectively). The surface morphology and chemical composition of the as-prepared coatings were characterized by a scanning electron microscope (SEM), an X-ray energy dispersive spectroscopy (EDS), a Fourier-transform infrared spectroscopy (FT-IR) and an X-ray photoelectron spectroscopy (XPS). The water contact angles, chemical stability, corrosion resistance and self-cleaning of the as-prepared coatings were investigated by a water contact angle measurement and electrochemical workstation. The results showed that the component of the as-prepared coatings was nickel stearate, and the surface morphologies of the coatings were closely correlated with the deposition time. In the initial stage, nickel ions (Ni^{2+}) reacted with stearate ions ($\text{CH}_3(\text{CH}_2)_{16}\text{COO}^-$) to form nano sheet-shape nickel stearate on the surface of copper substrate. As the deposition time increased, the nano sheets gradually increased and interconnected each other, eventually formed micro-scale flower-like structures. So, the surface morphology of nickel stearate changed from uniform nano sheets (10 min) to scattered flower-like structures (30 min), and finally to uniform and dense flower-like structures (50 min). The wettability test showed that the water contact angle (θ_{WCA}) of NS-1 with nano sheet-like structures was only about $(130.7 \pm 2.2)^\circ$. The θ_{WCA} of scattered flower-like NS-2 was improved to $(147.8 \pm 2.5)^\circ$ due to the increase of surface roughness. The NS-3 exhibited desirable superhydrophobicity with a θ_{WCA} of $(157.3 \pm 1.9)^\circ$ and a θ_{SA} of $(3.6 \pm 1.1)^\circ$ when the surface was covered by uniform and dense hierarchical micro/nano-scaled flower-like structures. Furthermore, different kinds of droplets (such as tea, methylene blue solution, methyl orange solution, milk, NaCl solution and coke) on NS-3 surface maintained a spherical shape with the WCAs ranging between 154.3° and 156.5° , indicating that the NS-3 surface had excellent superhydrophobicity and antifouling properties. Clearly, the coarse hierarchical structure had a better ability to trap a large amount of air and improve the superhydrophobicity compared with the nano sheet-like structure. The stability test found that WCA of the superhydrophobic NS-3 coating maintained larger than 152.1° and the RAs values maintained lower than 7° when the pH values ranged from 1 to 14, indicating that pH had little effect on the WCAs. The NS-3 coating still possessed good superhydrophobic performance with a WCA of 151.8° after soaking for 8 days in 3.5wt.% NaCl solution. These phenomena indicated that the superhydrophobic NS-3 coating had outstanding chemical stability. Tafel tests showed that the J_{corr} of NS-3 superhydrophobic surface were $1.75 \times 10^{-6} \text{ A/cm}^2$, which was decreased about 7 and 20 times, respectively, in comparison with NS-2 and NS-1. For the self-cleaning test, the spherical droplets quickly rolled off and took away the surface contaminants (such as graphite powder, SiO_2 powder and SiC powder). It could be anticipated that the micro/nano hierarchical structured NS-3 showed excellent superhydrophobicity, self-cleaning, chemical stability and corrosion resistance. Using deep eutectic solvent as the electrolyte provides a promising method to fabricate micro/nano hierarchical structured superhydrophobic surface by one-step electrodeposition method.

KEY WORDS: deep eutectic solvent; electrodeposition; nickel stearate; micro/nano hierarchical structure; superhydrophobicity; corrosion resistance; self-cleaning

得益于特殊的表面浸润特性,超疏水材料在自清洁^[1-2]、防结冰^[3-4]、油水分离^[5-6]、金属防腐^[7-8]等领域表现出广阔的应用前景。研究表明,表面粗糙度和表面自由能是决定材料超疏水性的两个主要因素。经过十几年的发展,科研人员已开发出一系列制备超疏水表面的方法^[9-14],如激光刻蚀法、3D 打印法、静电纺丝法、化学气相沉积法、溶胶-凝胶法、自组装法以及电沉积法等。在上述方法中,电沉积法由于具有设备及操作简单、沉积速度快、易于控制、成本低以及通过改变电沉积参数即可实现对材料表面形貌的

多样化调控等优点,被广泛用于超疏水材料的制备。

电沉积法制备超疏水表面主要有以下两种方法:一是先采用电沉积技术在基底表面沉积一层粗糙结构,然后再在其表面修饰一层低表面能物质;二是将低表面能物质,如硬脂酸、十四酸等长链脂肪酸和金属盐一起溶解到电解液中,通过一步电沉积构筑具有粗糙结构的低表面能表面。两种方法相比,两步法更易得到粗糙的微纳分级结构,但表面的低表面能层却很容易遭到破坏;而一步法则具有简单、高效且制备的镀层自身具备低表面能特性。目前已报道的一步电

沉积法制备超疏水镀层通常是在水/乙醇溶液体系进行的。虽然科研人员通过优化沉积电压、沉积时间或电解液组成等参数制备得到一系列性能优异的超疏水金属镀层,如十四酸铜^[15]、十四酸铈^[16]、十四酸镧^[17]、十四酸铁^[18]、硬脂酸铜^[19]、硬脂酸锰^[20]、棕榈酸锰^[21]等,但如何通过一步电沉积法构筑具有微纳分级结构的表面仍然是人们研究的热点。与水溶液相比,低共熔溶剂具有宽的电化学窗口、高的金属盐溶解性、高的电导率、无析氢以及易沉积得到纳米晶沉积物等优点,在电化学沉积和纳米材料制备方面受到广泛应用^[22-23]。此外,十四酸、硬脂酸等难溶于水的低表面能物质可直接溶于低共熔溶剂,通过调节沉积参数即可实现镀层微纳分级结构和低表面能组分的同步调控。Liang 团队在低共熔溶剂体系电沉积制备超疏水金属镀层方面开展了大量研究^[24-28],采用先电沉积构筑粗糙结构层再浸泡或电沉积修饰低表面能层的方法,通过调控电解液组成、沉积电流、沉积时间等制备得到一系列具有优异油水分离特性、耐腐蚀性以及不同粘附特性的超疏水镀层。然而,目前以低共熔溶剂为电解液制备超疏水镀层通常采用两步法,关于低共熔溶剂中一步电沉积制备同时具备微纳分级结构和低表面自由能的镀层的研究鲜有报道。

基于以上分析,采用氯化胆碱-尿素低共熔溶剂替代水溶液,向其中添加一定比例的六水氯化镍和硬脂酸溶解后得到电解液,采用一步电沉积法制备超疏水硬脂酸镍镀层。研究了低共熔溶剂体系中电沉积时间对镀层表面形貌的影响,考察了所制备超疏水镀层的超疏水性、自清洁性及耐腐蚀性能。

1 试验

1.1 超疏水镀层的制备

氯化胆碱 (C₅H₁₄ClNO, ChCl, AR)、尿素 (CH₄N₂O, AR)、氯化镍 (NiCl₂·6H₂O, AR)、硬脂酸 (C₁₈H₃₆O₂, AR)、氯化钠 (NaCl, AR) 均购自西陇科学股份有限公司。称取 100 g 氯化胆碱和 86 g 尿素加入烧杯,在 80 ℃ 下充分搅拌溶解得到无色透明的低共熔溶剂。向上述低共熔溶剂中依次加入 0.04 mol/L 的六水氯化镍和 0.1 mol/L 的硬脂酸粉末并充分搅拌至完全溶解。

电沉积试验以镍片为阳极,铜片为阴极,两者间距 4 cm。电沉积开始前,选用 600 目、1 000 目、1 500 目砂纸对铜片进行打磨去除表面氧化膜,然后再经丙酮溶液超声除油、稀盐酸溶液活化处理,最后用蒸馏水清洗干净并吹干。电沉积采用一步恒压法,沉积电压为 3 V,沉积温度为 80 ℃,搅拌速率为 300 r/min,沉积时间分别为 10、30、50 min。为了便于讨论,根据沉积时间由小到大,将所制备的硬脂酸镍 (Nickel Stearate) 镀层依次命名为 NS-1、NS-2 和 NS-3。

1.2 样品表征

采用扫描电子显微镜 (FESEM, Carl Zeiss, Sigma 500) 研究了不同沉积时间下制备镀层的形貌结构,采用 X 射线能谱仪 (EDS)、傅里叶变换红外光谱仪 (FTIR, Thermo Scientific, Nicolet iS50) 以及 X 射线光电子能谱仪 (XPS, Kratos, Axis-Ultra DLD-600 W) 对所制备镀层成分进行了表征。为了研究所制备镀层的超疏水性,利用接触角测量仪 (上海中晨, JC2000D1) 测量其静态接触角。为了考察所制备样品的耐腐蚀性,利用电化学工作站 (上海辰华, CHI660E) 进行动电位极化曲线 (Tafel) 测试。测试参数如下:测试采用传统的三电极体系,样品、铂片和饱和甘汞电极分别为工作电极、对电极和参比电极,腐蚀液为 3.5% NaCl 溶液,扫描范围为-1.2~0.4 V,扫速为 0.01 V/s。为了获得稳定的开路电位,电化学测试前样品需静置 30 min。

2 结果及分析

2.1 镀层表面形貌和组分

表面微纳结构和表面自由能是构筑超疏水材料的 2 个重要因素。表 1 给出了 3 种镀层的元素组成 (EDS),由表可知,不同时间下制备的样品都含有碳、氧、镍 3 种元素,且 3 个样品中碳氧镍含量的相对比值 (C : O : Ni=7.3 : 1.1 : 1) 与硬脂酸镍中元素比完全吻合,这说明所制备镀层为硬脂酸镍 (Ni[CH₃(CH₂)₁₆COO]₂)。图 1 给出了不同沉积时间下制备镀层的低倍 (×5 000) 和高倍 (×35 000) 形貌。由图 1a 可知,当沉积时间为 10 min 时,所制备镀层表面相对平整,高倍下可以看到纳米尺度的片状物分布在镀层表面。随着沉积时间的延长 (30 min, 图 1b),镀层表面片状物数量增加,部分片状物相互堆积形成少量微米尺度的花状突起,零星的分布在镀层表面,镀层粗糙度增大。当沉积时间增加到 50 min (图 1c),镀层表面被大量花状突起均匀覆盖;由高倍电镜可以看到,每个微米尺度的花状突起 (1~3 μm) 是由大量纳米尺度的片状物堆积而成,呈现出花状微纳分级结构。这说明在氯化胆碱-尿素低共熔溶剂中,通过优化沉积时间在铜基底表面成功制备得到具有较高粗糙度的微纳分级结构。

表 1 镀层的元素组成及含量			
Tab.1 Elemental composition and content of coatings			
wt. %			
Specimens	Ni	C	O
NS-1	10.54	77.89	11.57
NS-2	10.57	77.81	11.62
NS-3	10.65	77.63	11.72

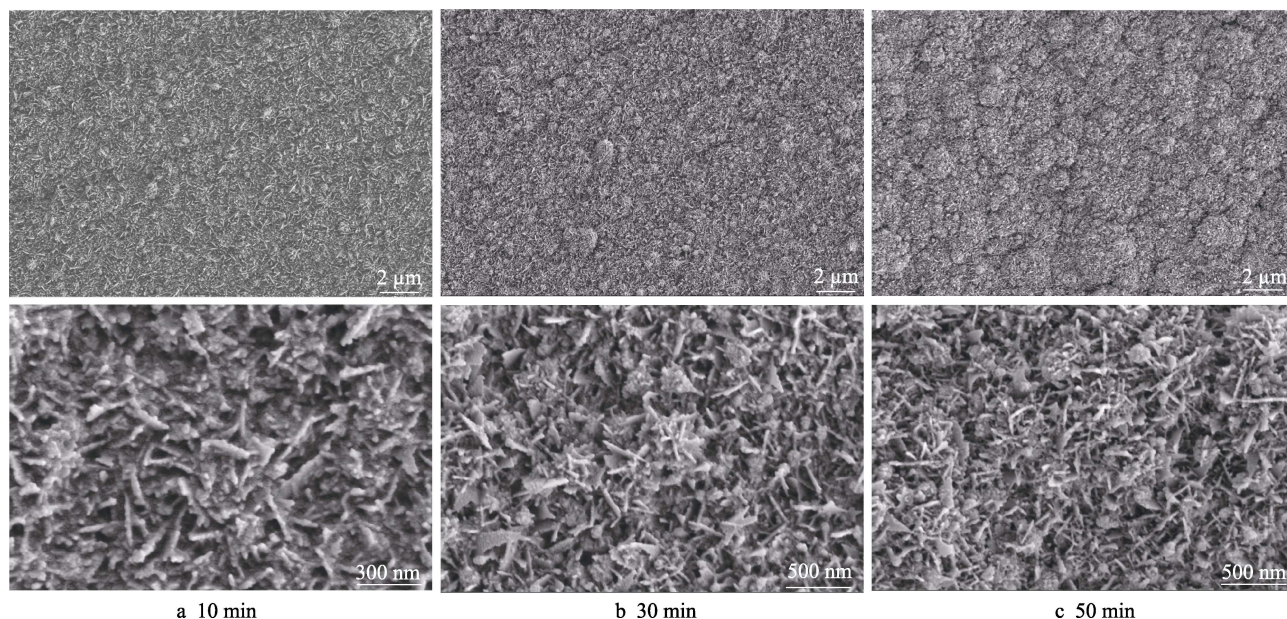


图1 不同沉积时间制备镀层的表面形貌

Fig.1 Morphologies of as-prepared coatings deposited at different time

为了探究所制备镀层的表面化学组成,图2给出了硬脂酸和NS-3的傅里叶变换红外光谱图(FTIR)。在硬脂酸的红外光谱图中,在 2917 cm^{-1} 和 2849 cm^{-1} 处出现的2个吸收峰分别归属于亚甲基($-\text{CH}_2$)的不对称伸缩振动和对称伸缩振动^[20],而 1701 cm^{-1} 处的尖锐峰则属于硬脂酸中羧基($-\text{COOH}$)的振动吸收峰。与硬脂酸的FTIR一样,NS-3红外光谱图的 2915 cm^{-1} 和 2847 cm^{-1} 处也出现了 $-\text{CH}_2$ 的不对称伸缩振动和对称伸缩振动峰,这表明NS-3表面组成中含有长链脂肪族基团。与硬脂酸不同的是,NS-3的红外光谱图中 1701 cm^{-1} 处并没有出现 $-\text{COOH}$ 的振动吸收峰,但在 1537 cm^{-1} 和 1463 cm^{-1} 处出现了羧酸根($-\text{COO}^-$)的不对称伸缩振动峰和对称伸缩振动峰^[29],这说明所制备镀层的表面成分为硬脂酸盐,与EDS结论相吻合。

为了进一步证实所制备镀层的化学成分,图3给出了NS-3镀层的XPS全谱以及C 1s、O 1s和Ni 2p的高分辨率光谱。由XPS全谱(图3a)可知,镀层由C、O、Ni 3种元素组成。C 1s高分辨率光谱(图3b)可拟合为3个峰,结合能在 284.68 、 285.28 、 288.38 eV 处的特征峰分别对应于 $-\text{CH}_2$ 、 $-\text{CH}_3$ 和 $\text{O}=\text{C}-\text{O}$ 基团。NS-3镀层的O 1s的高分辨率光谱(图3c)可拟合为2个峰,结合能在 531.48 eV 和 532.28 eV 处的峰分别归属于C—O和C=O基团。由Ni 2p的高分辨率光谱(图3d)可以看出,在 845 eV 到 890 eV 范围内出现的4个Ni 2p峰均属于 Ni^{2+} ^[30]:结合能在 855.98 eV 和 860.78 eV 处的特征峰分别对应于O—Ni基团的Ni 2p_{3/2}特征峰和及其伴峰,结合能在 873.48 eV 和 880.58 eV 处的特征则分别对应于O、—Ni基团的Ni 2p_{1/2}的特征峰及其伴峰。XPS结果进

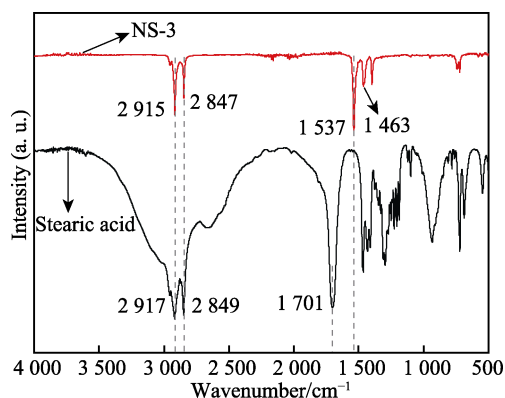


图2 硬脂酸和NS-3镀层红外光谱图

Fig.2 FTIR of stearic acid and NS-3 coatings

一步证实电沉积镀层为硬脂酸镍。

2.2 电沉积过程

基于镀层表面形貌及成分分析,图4给出了花状硬脂酸镍的电沉积示意图。低共熔溶剂中硬脂酸盐形成机理与水溶液中硬脂酸盐形成机理相同^[17,21]。初始阶段,溶解在低共熔溶剂中的硬脂酸根离子和镍离子在阴极表面反应生成纳米尺度的片状硬脂酸镍。随着沉积的进行,片状硬脂酸镍的数量和尺寸不断增加,在阴极表面形成一层均匀致密的片状结构的硬脂酸镍层。当沉积时间达到 30 min 时,部分片状硬脂酸镍相互交叉、堆积形成微米尺度的花状突起,此时的镀层表面整体呈现零散分布的花状突起。随着沉积继续进行,花状突起的数量逐渐增多,当沉积时间增加到 50 min 时,镀层表面呈现出均匀致密的花状突起结构。每个微米尺度的花状突起由大量纳米尺度的片状硬脂酸镍相互堆积而成,从而赋予表面粗糙的微纳分级结构。因此,在含有氯化镍和硬脂酸的低共熔溶

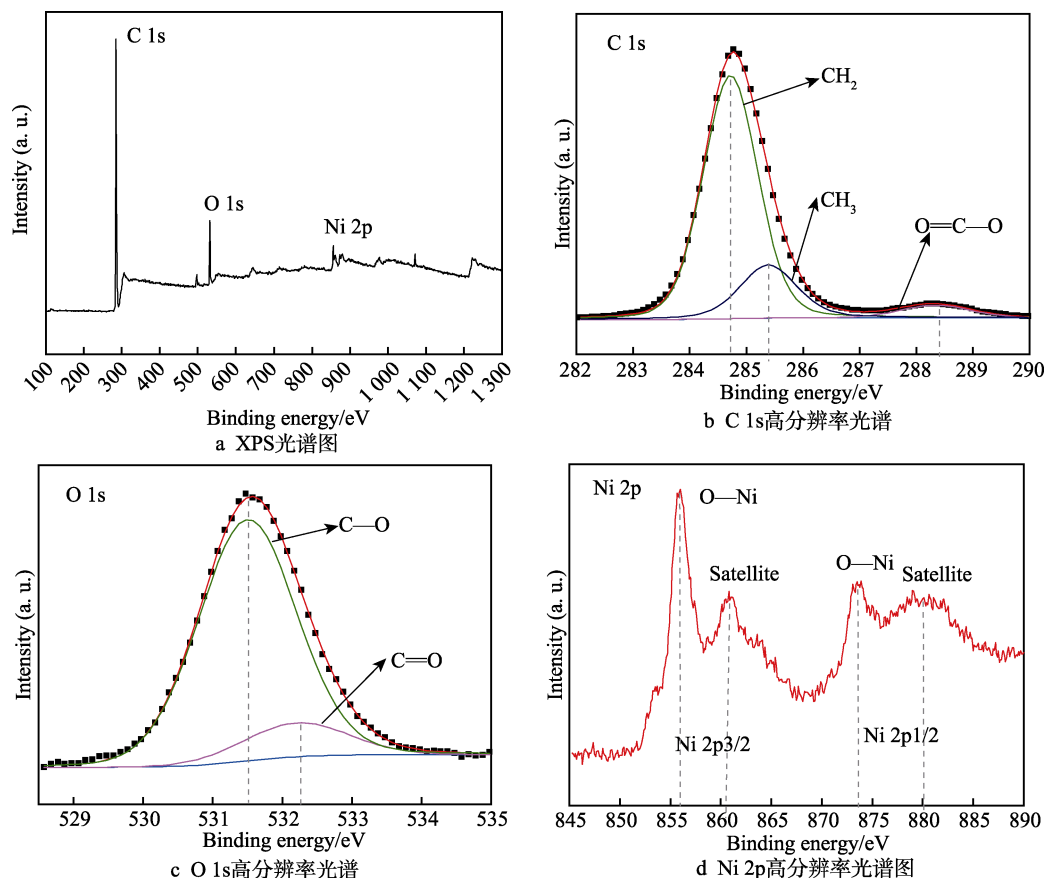


图 3 NS-3 镀层的 (a) XPS 光谱图, (b) C 1s 高分辨率光谱,

(c) O 1s 高分辨率光谱和 (d) Ni 2p 高分辨率光谱图

Fig.3 XPS spectrum of NS-3 coatings (a), high-resolution XPS spectra of C 1s (b), O 1s (c) and Ni 2p (d)

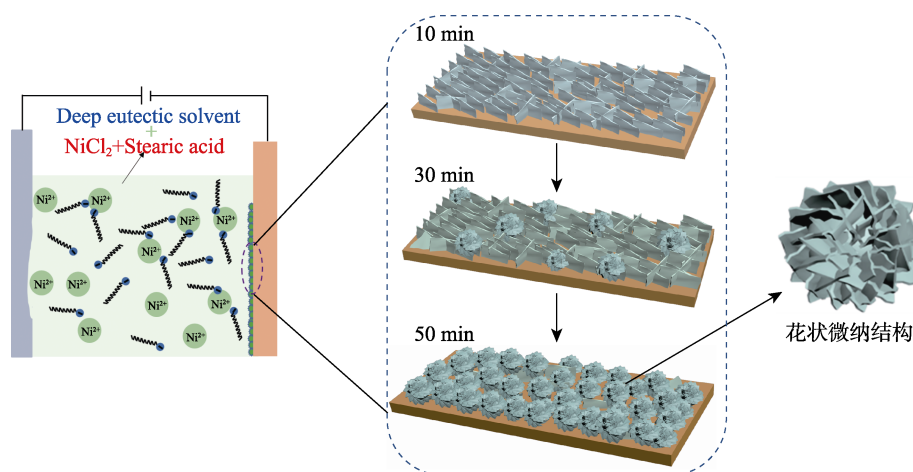


图 4 花状微纳分级结构硬脂酸镍电沉积示意图

Fig.4 Electrodeposition schematics of nickel stearate with flower-like hierarchical structures

剂体系中, 通过一步电沉积制备得到同时具有微纳分级结构和低表面能特性的硬脂酸镍镀层。

2.3 超疏水性和稳定性

图 5a 给出了不同沉积时间下制备的硬脂酸镍镀层的静态接触角 (θ_{WCA})。尽管 3 种硬脂酸镍镀层都

具有相同的低表面能特性, 却表现出不一样的浸润特性。由于 NS-1 镀层表面粗糙度较低, 其接触角仅为 $(130.7 \pm 2.2)^\circ$ 。随着沉积时间增加 (30 min), 镀层表面纳米尺度片状物和微米尺度花状突起数量增加, 表面粗糙度提高, NS-2 的接触角增加到 $(147.8 \pm 2.5)^\circ$, 开始呈现出超疏水特性。当沉积时间增加到 50 min

时,得益于表面粗糙的微纳分级结构和自身低表面能特性,NS-3 镀层接触角高达 $(157.3\pm 1.9)^\circ$,滚动角为 $(3.6\pm 1.1)^\circ$,表现出优异的超疏水特性。很显然,3种硬脂酸镍镀层接触角的差异主要归因于其表面结构(粗糙度)的不同。为了考察超疏水 NS-3 镀层对不同液滴的疏水性,图 5b 给出了不同液滴在 NS-3 镀层表面的接触角和浸润性照片。由图 5b 可以看出,茶水、亚甲基蓝溶液、甲基橙溶液、牛奶、盐水以及可乐等液滴在 NS-3 镀层表面均呈现球形,而且所有液滴接触角均大于 $(154.3\pm 0.9)^\circ$ 。这说明 NS-3 镀层不仅对蒸馏水,对其他液滴也具有优异的超疏水效果,其超疏水性具有普适性。

化学稳定性是评价超疏水材料的一个重要性能指标。图 6a 给出了 NS-3 镀层浸泡在不同 pH 值溶液中 12 h 前后的接触角变化。由图可知,浸泡前不同 pH 值的液滴在 NS-3 镀层表面接触角均大于 152° ,即使在强酸($\text{pH}=1$, $\theta_{\text{WCA}}=152.1^\circ$)和强碱($\text{pH}=14$, $\theta_{\text{WCA}}=152.3^\circ$)条件下也表现出超疏水特性。经过 12 h 浸泡后,NS-3 镀层的接触角出现轻微的下降,但仍然高于 150° 。图 6b 给出了 NS-3 超疏水镀层浸泡在 3.5% NaCl 溶液一段时间后的接触角变化。由图 6b

可以看出,浸泡 5 d 后,NS-3 镀层的接触角和滚动角几乎没有发生变化。当浸泡 10 d 后,NS-3 镀层接触角仍然大于 151.2° ,对应滚动角小于 8° 。这说明 NS-3 超疏水镀层对强酸、强碱及盐水溶液具有较好的化学稳定性^[16,21,25]。

2.4 耐腐蚀性和自清洁性

为了考察所制备超疏水镀层的耐腐蚀性能,图 7 给出了 3 个样品在 3.5% NaCl 溶液中的动电位极化曲线,并利用塔菲尔外推法得到 3 种硬脂酸镀层的电化学腐蚀参数(表 2)。如图 7 所示,随着沉积时间的增加,硬脂酸镍镀层的腐蚀电位正移,腐蚀电流密度显著降低,说明其耐腐蚀性能逐渐提高。由表 2 可知,与 NS-1 相比($J_{\text{corr}}=3.56\times 10^{-5}\text{ A/cm}^2$),NS-2 和 NS-3 镀层的腐蚀电流密度分别降低了 7 倍和 20 倍。NS-3 优异的耐腐蚀性能与其表面花状微纳分级结构密切相关:首先,大量空气填充在粗糙的微纳分级结构之间并在固/液界面之间形成一层空气垫,显著降低了腐蚀介质与镀层的接触面积^[21];其次,固/液界面之间的空气垫作为物理屏障可有效抑制腐蚀离子进入及电荷转移^[19]。

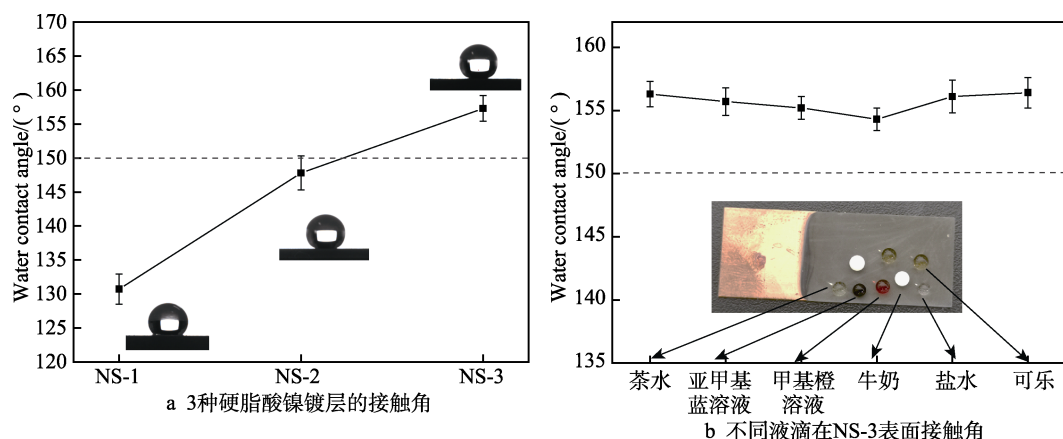


图 5 3 种硬脂酸镍镀层的接触角 (a) 及不同液滴在 NS-3 表面接触角 (b)
Fig.5 Contact angles of three nickel stearate coatings (a) and different droplets on NS-3 surfaces (b)

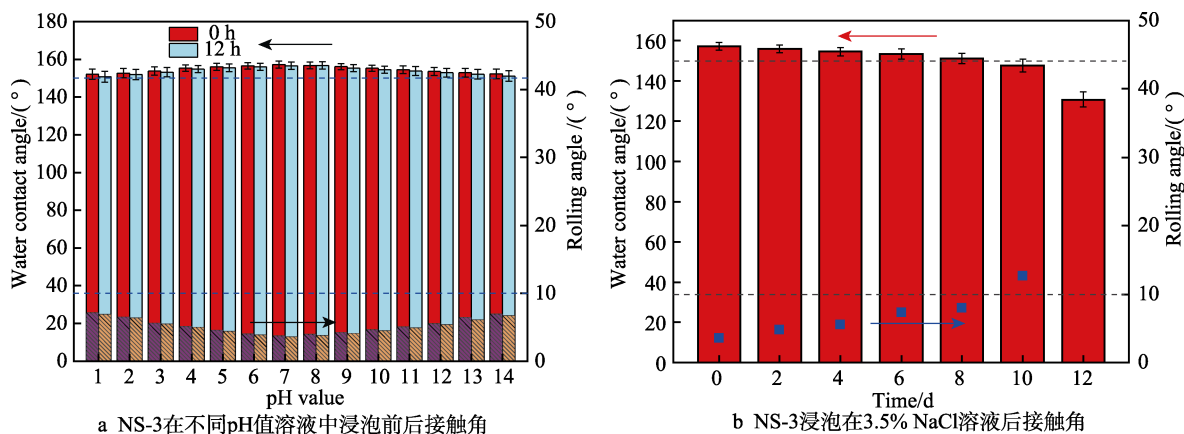


图 6 NS-3 镀层的化学稳定性
Fig.6 Chemical stability of NS-3 coatings

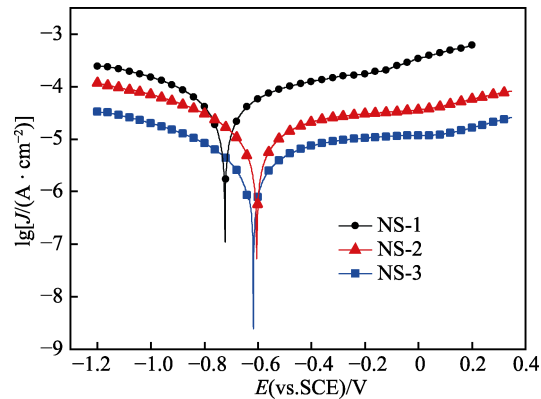


图 7 NS-3 镀层在 3.5% NaCl 溶液中的 Tafel 曲线
Fig.7 Tafel curves of NS-3 coatings in 3.5wt.% NaCl solution

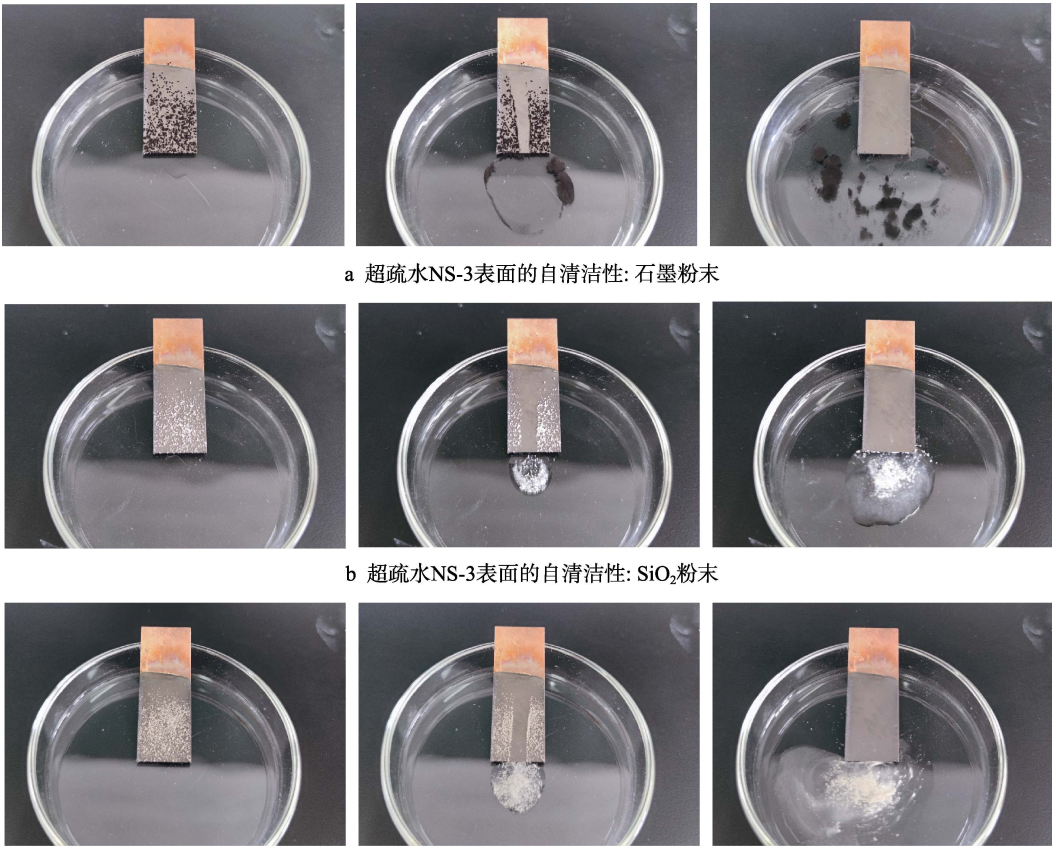
自清洁性是低粘附超疏水材料的一个重要性能。以石墨粉末、二氧化硅粉末和碳化硅粉末模拟灰尘，

研究了 NS-3 超疏水镀层对上述 3 种污染物的自清洁效果。由图 8 可以看出,得益于其优异的超疏水特性,当把蒸馏水滴到撒有石墨粉、二氧化硅粉末以及碳化硅粉末等污染物的 NS-3 镀层表面时,能迅速形成球形水滴,并裹挟着污染物一起滚落,并在镀层表面形成一条干净的轨迹;随着水滴的持续滴落,镀层表面的污染物被完全冲洗干净。这表明花状微纳分级结构可以赋予硬脂酸镍镀层优异的自清洁特性,甚至在表面沾有灰尘的情况下仍可保持超疏水特性。

表 2 硬脂酸镍镀层的电化学腐蚀参数

Tab.2 Electrochemical corrosion data of nickel stearate coatings

Specimens	E_{corr} (vs. SCE)/V	$J_{\text{corr}}/(\text{A} \cdot \text{cm}^{-2})$
NS-1	-0.76	3.56×10^{-5}
NS-2	-0.57	5.14×10^{-6}
NS-3	-0.60	1.75×10^{-6}



a 超疏水NS-3表面的自清洁性: 石墨粉末

b 超疏水NS-3表面的自清洁性: SiO₂粉末

c 超疏水NS-3表面的自清洁性: SiC 粉末

图 8 NS-3 镀层表面自清洁测试
Fig.8 Self-cleaning test of NS-3 coatings

3 结论

1)硬脂酸镍镀层表面形貌与沉积时间密切相关。随沉积时间增加,镀层表面形貌由均匀的纳米片状结构变为零星的花状突起结构,最终形成均匀致密的微

纳分级结构的花状突起结构。

2)得益于独特的花状微纳分级结构和自身低表面能特性, NS-3 镀层不仅表现出超疏水性 ($\theta_{\text{WCA}}=(157.3\pm1.9)^{\circ}$, $\theta_{\text{SA}}=(3.6\pm1.1)^{\circ}$)、耐腐蚀性 ($J_{\text{corr}}=1.75\times10^{-6}\text{ A/cm}^2$) 和自清洁特性,对强酸、强碱及盐水溶液还表现出优异的化学稳定性。

3) 以低共熔溶剂为电解液可实现具有微纳分级结构表面的快速、可控构筑, 对高性能超疏水镀层的大规模制备及工业化应用具有重要意义。

参考文献:

- [1] LU Chen-xi, GAO Yuan, YU Sen-jiang, et al. Non-Fluorinated Flexible Superhydrophobic Surface with Excellent Mechanical Durability and Self-Cleaning Performance[J]. ACS Applied Materials & Interfaces, 2022, 14(3): 4750-4758.
- [2] 陈枫, 胡泽顺, 姚镇城, 等. 环保超疏水防潮瓦楞纸箱的制备及性能研究[J]. 包装工程, 2022, 43(9): 46-50.
CHEN Feng, HU Ze-shun, YAO Zhen-cheng, et al. Preparation and Performance of Environmentally Friendly Super-hydrophobic and Moisture-proof Corrugated Box[J]. Packaging Engineering, 2022, 43(9): 46-50.
- [3] KORCZENIEWSKI E, BRYK P, KOTER S, et al. Are Nanohedgehogs Thirsty? Toward New Superhydrophobic and Anti-Icing Carbon Nanohorn-Polymer Hybrid Surfaces [J]. Chemical Engineering Journal, 2022, 446: 137126.
- [4] HUANG Wei, HUANG Jin-xia, GUO Zhi-guang, et al. Icephobic/Anti-Icing Properties of Superhydrophobic Surfaces[J]. Advances in Colloid and Interface Science, 2022, 304: 102658.
- [5] PANG Yao, YU Zong-xue, CHEN Hai-dong, et al. Superhydrophobic Polyurethane Sponge Based on Sepiolite for Efficient Oil/Water Separation[J]. Journal of Hazardous Materials, 2022, 434: 128833.
- [6] CHENG Xi-quan, JIAO Yang, SUN Ze-kun, et al. Constructing Scalable Superhydrophobic Membranes for Ultra-fast Water-Oil Separation[J]. ACS Nano, 2021, 15(2): 3500-3508.
- [7] LIU Zhan-jian, ZHANG Cong-yuan, JING J, et al. Bristle Worm Inspired Ultra-Durable Superhydrophobic Coating with Repairable Microstructures and Anti-Corrosion/Scaling Properties[J]. Chemical Engineering Journal, 2022, 436: 135273.
- [8] 蒋帆, 赵越, 胡吉明. 超疏水表面在金属防护中应用的研究进展[J]. 表面技术, 2020, 49(2): 109-123.
JIANG Fan, ZHAO Yue, HU Ji-ming. Research Advance in Application of Superhydrophobic Surfaces in Corrosion Protection of Metals[J]. Surface Technology, 2020, 49(2): 109-123.
- [9] ZHANG Wen-luan, WANG De-hui, SUN Zheng-nan, et al. Robust Superhydrophobicity: Mechanisms and Strategies[J]. Chemical Society Reviews, 2021, 50(6): 4031-4061.
- [10] 佟威, 熊党生. 仿生超疏水表面的发展及其应用研究进展[J]. 无机材料学报, 2019, 34(11): 1133-1144.
TONG Wei, XIONG Dang-sheng. Bioinspired Superhydrophobic Materials: Progress and Functional Application [J]. Journal of Inorganic Materials, 2019, 34(11): 1133-1144.
- [11] 曾宪光, 黄茜, 彭静, 等. 电沉积法制备超疏水涂层的研究进展[J]. 腐蚀与防护, 2020, 41(10): 1-6, 73.
ZENG Xian-guang, HUANG Xi, PENG Jing, et al. Research Progress of Super-Hydrophobic Coating Prepared by Electro-Deposition[J]. Corrosion & Protection, 2020, 41(10): 1-6, 73.
- [12] 闫德峰, 刘子艾, 潘维浩, 等. 多功能超疏水表面的制造和应用研究现状[J]. 表面技术, 2021, 50(5): 1-19.
YAN De-feng, LIU Zi-ai, PAN Wei-hao, et al. Research Status on the Fabrication and Application of Multifunctional Superhydrophobic Surfaces[J]. Surface Technology, 2021, 50(5): 1-19.
- [13] 吴春亚, 黄俊杰, 李曦光, 等. 金属基超疏水表面的制备技术研究新进展[J]. 哈尔滨工业大学学报, 2021, 53(7): 1-19.
WU Chun-ya, HUANG Jun-jie, LI Xi-guang, et al. New Progress of Fabrication Techniques for Metal-Based Superhydrophobic Surfaces[J]. Journal of Harbin Institute of Technology, 2021, 53(7): 1-19.
- [14] SAM E K, SAM D K, LV Xiao-meng, et al. Recent Development in the Fabrication of Self-Healing Superhydrophobic Surfaces[J]. Chemical Engineering Journal, 2019, 373: 531-546.
- [15] 赵婷婷, 康志新, 马夏雨. 一步电沉积法制备超疏水 Cu 网及其耐腐蚀和油水分离性能[J]. 金属学报, 2018, 54(1): 109-117.
ZHAO Ting-ting, KANG Zhi-xin, MA Xia-yu. Fabricating Superhydrophobic Copper Meshes by One-Step Electrodeposition Method and Its Anti-Corrosion and Oil-Water Separation Abilities[J]. Acta Metallurgica Sinica, 2018, 54(1): 109-117.
- [16] LIU Qin, CHEN De-xin, KANG Zhi-xin. One-Step Electrodeposition Process to Fabricate Corrosion-Resistant Superhydrophobic Surface on Magnesium Alloy[J]. ACS Applied Materials & Interfaces, 2015, 7(3): 1859-1867.
- [17] ZHANG Yong-hui, LIU Jiang-wen, OUYANG Li-geng, et al. One-Step Preparation of Robust Superhydrophobic Foam for Oil/Water Separation by Pulse Electrodeposition[J]. Langmuir, 2021, 37(23): 7043-7054.
- [18] LI Bing-zhi, OUYANG Yi-bo, HAIDER Z, et al. One-Step Electrochemical Deposition Leading to Superhydrophobic Matrix for Inhibiting Abiotic and Microbiologically Influenced Corrosion of Cu in Seawater Environment[J]. Colloids and Surfaces A: Physicochemical and Engineering Aspects, 2021, 616: 126337.
- [19] WANG Han, DONG Shu-liang, WANG Zhen-long. One-Step Fabrication of Superhydrophobic Surface on Beryllium Copper Alloys and Corrosion Protection Application[J]. Colloids and Surfaces A: Physicochemical and Engineering Aspects, 2018, 556: 291-298.
- [20] ZHANG Bin-bin, LI Jia-run, ZHAO Xia, et al. Biomimetic one Step Fabrication of Manganese Stearate Superhydrophobic Surface as an Efficient Barrier Against

- Marine Corrosion and *Chlorella Vulgaris*-Induced Biofouling[J]. Chemical Engineering Journal, 2016, 306: 441-451.
- [21] ZHANG Bin-bin, XU Wei-chen, ZHU Qing-jun, et al. Ultrafast one Step Construction of Non-Fluorinated Superhydrophobic Aluminum Surfaces with Remarkable Improvement of Corrosion Resistance and Anti-Contamination[J]. Journal of Colloid and Interface Science, 2018, 532: 201-209.
- [22] HANSEN B B, SPITTLE S, CHEN B, et al. Deep Eutectic Solvents: A Review of Fundamentals and Applications[J]. Chemical Reviews, 2021, 121(3): 1232-1285.
- [23] CHEN Jia, ALI M C, LIU Rui-rui, et al. Basic Deep Eutectic Solvents as Reactant, Template and Solvents for Ultra-Fast Preparation of Transition Metal Oxide Nanomaterials[J]. Chinese Chemical Letters, 2020, 31(6): 1584-1587.
- [24] LI Rui-qian, GAO Qiao-hui, DONG Qiu-jing, et al. Template-Free Electrodeposition of Ultra-High Adhesive Superhydrophobic Zn/Zn Stearate Coating with Ordered Hierarchical Structure from Deep Eutectic Solvent[J]. Surface and Coatings Technology, 2020, 403: 126267.
- [25] 于会珠, 崔偲偲, 白子龙, 等. 微纳分级结构超疏水金属表面的电沉积构筑及性能[J]. 中国表面工程, 2021, 34(5): 181-187.
- YU Hui-zhu, CUI Wei-wei, BAI Zi-long, et al. Electrodeposition and Properties of Micro/Nanoscale Hierarchical Structured Superhydrophobic Metal Surface[J]. China Surface Engineering, 2021, 34(5): 181-187.
- [26] HOU Yuan-yuan, LI Rui-qian, LIANG Jun. Superhydrophilic Nickel-Coated Meshes with Controllable Pore Size Prepared by Electrodeposition from Deep Eutectic Solvent for Efficient Oil/Water Separation[J]. Separation and Purification Technology, 2018, 192: 21-29.
- [27] HOU Yuan-yuan, PENG Zhen-jun, LIANG Jun, et al. Facile Preparation of Petaliform-Like Superhydrophobic Meshes via Moisture Etching for Oil-Water Separation[J]. Surface and Coatings Technology, 2020, 399: 126124.
- [28] HOU Yuan-yuan, PENG Zhen-jun, LIANG Jun, et al. Robust and Non-Fluorinated Superhydrophobic Meshes with Controllable Pore Size for High-Efficiency Water-in-Oil Emulsion Separation[J]. Separation Science and Technology, 2021, 56(10): 1699-1709.
- [29] LIU Yan, XUE Jing-ze, LUO Dan, et al. One-Step Fabrication of Biomimetic Superhydrophobic Surface by Electrodeposition on Magnesium Alloy and Its Corrosion Inhibition[J]. Journal of Colloid and Interface Science, 2017, 491: 313-320.
- [30] LI Rui-qian, HOU Yuan-yuan, LIANG Jun. Electro-Codeposition of Ni-SiO₂ Nanocomposite Coatings from Deep Eutectic Solvent with Improved Corrosion Resistance[J]. Applied Surface Science, 2016, 367: 449-458.

责任编辑: 万长清

(上接第 305 页)

- [12] ZHANG Zhao-qing, SHI Kai-ning, HUANG Xin-chun, et al. Development of a Probabilistic Algorithm of Surface Residual Materials on Si₃N₄ Ceramics under Longitudinal Torsional Ultrasonic Grinding[J]. Ceramics International, 2022, 48(9): 12028-12037.
- [13] GAO G F, ZHAO B, XIANG D H, et al. Research on the Surface Characteristics in Ultrasonic Grinding Nano-Zirconia Ceramics[J]. Journal of Materials Processing Technology, 2009, 209(1): 32-37.
- [14] YOUNIS M A, ALAWI H. Probabilistic Analysis of the Surface Grinding Process[J]. Transactions of the Canadian Society for Mechanical Engineering, 1984, 8(4): 208-213.
- [15] XU H H K, JAHANMIR S, IVES L K. Effect of Grinding on Strength of Tetragonal Zirconia and Zirconia-Toughened Alumina[J]. Machining Science and Technology, 1997, 1(1): 49-66.
- [16] 李厦, 尤佳旗. 基于弹性变形的超声磨削氧化锆陶瓷的粗糙度模型[J]. 组合机床与自动化加工技术, 2017(11): 23-27.
- LI Sha, YOU Jia-qi. A Roughness Model of Zirconia Ceramic Based on Elastic Deflection in Ultrasonic Grinding[J]. Modular Machine Tool & Automatic Manufacturing Technique, 2017(11): 23-27.
- [17] 周云光. 镍基单晶高温合金微磨削工艺理论与关键技术研究[D]. 沈阳: 东北大学, 2017.
- ZHOU Yun-guang. Study on the Technological Theory and Key Technology in Micro Grinding Nickel-Based Single Crystal Superalloy[D]. Shenyang: Northeastern University, 2017.
- [18] YAMADA T, LEE H S, MIURA K. Effect of Contact Stiffness of Grinding Wheel on Ground Surface Roughness and Residual Stock Removal of Workpiece[J]. Advanced Materials Research, 2013, 797: 522-527.
- [19] YAN Yan-yan, ZHANG Zhao-qing, ZHAO Bo, et al. Study on Prediction of Three-Dimensional Surface Roughness of Nano-ZrO₂ Ceramics under Two-Dimensional Ultrasonic-Assisted Grinding[J]. The International Journal of Advanced Manufacturing Technology, 2021, 112(9-10): 2623-2638.
- [20] JIANG Jing-liang, GE Pei-qi, HONG Jun. Study on Micro-Interacting Mechanism Modeling in Grinding Process and Ground Surface Roughness Prediction[J]. The International Journal of Advanced Manufacturing Technology, 2013, 67(5): 1035-1052.

责任编辑: 万长清